Supporting Information

Weiße et al.

SI Materials and Methods

Cloning. Genomic DNA of *Candidatus Korarchaeum cryptofilum* was kindly provided by Dr. James G. Elkins (Oak Ridge National Laboratory, USA). The open reading frames (ORF) coding for a putative ACD alpha subunit (kcr_0198) and beta subunit (kcr_0115) were amplified by PCR. For kcr_0198 the primer pair 5′-CTTGGGATGCCATATGAACG-ACCTAGAGAGGC-3′ and 5′-GATGAACGTCTCGAGATCACCTCACGGCCAGG-3′ was used. For kcr_0115 the primer pair 5′-CGGTGATCATATGAGCTCAAGGGACC-3′ and 5′-CTTCCTCGAGAAGCCCTCACCTCAGG-3′ was used. Each primer pair contained restriction sites for the endonucleases NdeI and XhoI (underlined), which were used for insertion of the amplified ORF into pET17b to yield the expression vectors pET17bkcr_0198 and pET17bkcr_0115, respectively. Each vector was subsequently transformed into *E. coli* strain BL21(DE3) CodonPlus RIL (Stratagene).

Expression and purification. Recombinant *ckc*ACD1 was obtained by heterologous expression in *E. coli* BL21(DE3) CodonPlus RIL cells. Bacterial strains bearing either the expression plasmids encoding the alpha subunit (pET17bkcr_0198) or the beta subunit (pET17bkcr_0115) were independently cultivated in lysogenic broth (LB) media at 37 °C in presence of ampicillin and chloramphenicol. The following expression protocol was applied to each culture. At an optical density of 0.4 to 0.8 at 600 nm, expression was induced using IPTG to a final concentration of 0.4 mM. After a further cultivation period of 5 hours, cells were harvested by centrifugation and re-suspended in ACD buffer (100 mM TRIS/HCl, 150 mM NaCl and 5 mM $MgCl_2$ (final pH 7.5)). Cell lysis was performed by sonification. Cell debris was removed via centrifugation. The cleared lysates were incubated at 68 °C for 20 min to precipitate heat-labile proteins, which were pelleted by centrifugation. SDS-PAGE analysis was used to estimate the amount and purity of the target proteins. Reconstitution of the active *ckc*ACD1 heterotetramer was performed by mixing supernatants from both subunits, with the beta subunit in stoichiometric excess. The reconstituted *ckc*ACD1 complex was purified via gel filtration (Superdex 200 (GE Healthcare)) using ACD buffer for equilibration and protein elution. Due to a massive release of endogenous DNA during the lysis step, the eluted protein was contaminated with a high concentration of oligonucleotides. Multiple repeats of

purification via gel filtration were performed until UV spectra showed only protein specific absorption. Prior the final gel filtration step, the protein solution was incubated at 78 °C for 15 min. Purified *ckc*ACD1 was concentrated to 12.9 mg/ml as determined via UV absorption using a theoretical extinction coefficient of 49,280 $M^{-1}cm^{-1}$ calculated with the software tool PROTPARAM (1). Seleno-methionine labelled *ckc*ACD1 was produced with the following modifications for expression and purification. SelenoMethionine Medium Base supplemented with SelenoMethionine Medium Nutrient Mix (both Molecular Dimensions, Newmarket, United Kingdom) was used according to manufacturer's instructions (referred to as minimal medium in the following text). *E. coli* cells were cultured in this minimal medium with 50 mM methionine until an optical density of 0.4 at 600 nm was reached. At that point the cells were pelleted and re-suspended in pre-warmed minimal medium supplemented with 25 mM seleno-methionine. After a 20 min cultivation period, expression was induced with IPTG to a final concentration of 0.4 mM. The bacterial cells were harvested after 3 hours of cultivation. Essentially the same purification procedure as described for wild type *ckc*ACD1 was applied, with buffers additionally supplemented with 20 mM DTT.

Crystallisation. Initial crystallization experiments were performed at the HTX facility at the EMBL outstation (Hamburg, Germany) in sitting drop geometry. Crystals were obtained in various conditions, indicating two crystal forms according to their different optical appearance. Optimization of various parameters including pH, precipitation agent and concentration, crystallization temperature and droplet geometry were carried out to finally yield larger and well-formed crystals suitable for X-ray diffraction experiments. In order to obtain enzyme in complex with various substrates, the protein solution was usually supplemented with the appropriate cofactors. A magnesium ion-reduced protein solution was prepared by dialyzing against the 100-fold volume of 100 mM TRIS/HCl, 150 mM sodium chloride (final pH 7.5) using a membrane with 12 kDa MWCO. Dialysis was performed at 348 K. Precipitate was removed via centrifugation. Prior to further experiments the appropriate ligands and cofactors were added to the protein solution. Phosphorylated *ckc*ACD1 was obtained by either incubation with 10 mM ATP in ACD buffer for 2 min at 348 K or with 1 mM Ac-CoA in 10 mM Na_2HPO_4 and 5 mM sodium acetate for 1 min at 348 K using magnesium ion-reduced protein solution.

Diffraction experiments. Prior to any diffraction experiment the crystals were swiped through a cryo protection solution composed of 20 % (v/v) MPD and 80 % (v/v) mother liquor with 10 % higher concentration compared to the reservoir solution and eventually flash frozen in

liquid nitrogen. To avoid the washing out of bound ligands during this procedure, the ligands were added as well to the cryo buffer at the same concentration as in the crystallization droplet. X-Ray diffraction was performed at 100 K. Diffraction data were collected at various beamlines: ID23-1 at ESRF (Grenoble, France), beamlines BL14.1, BL14.2 and BL14.3 operated by the Helmholtz-Zentrum Berlin (HZB) at the BESSY II electron storage ring (Berlin-Adlershof, Germany)(2) and beamline P14 (MX2) at PETRA III (DESY, Hamburg, Germany). Diffraction images were indexed and scaled with XDS and XSCALE (3). Merging of reflections was done using AIMLESS (4).

Phasing and structure refinement. The crystallographic phase problem was solved using molecular replacement. A molecular model for the alpha subunit with the correct amino acid annotation was automatically generated by the SWISS-MODEL server (5) using the crystal structure of PH0766 from *Pyrococcus horikoshii* OT3 (PDB entry 2CSU) as template structure. For the beta subunit a model automatically built within MOLREP (6) based on PDB entry 1WR2 by providing the target amino acid sequence. Placement of the subunits was calculated using MOLREP and software from the PHENIX suite (7). Refinement of the crystal structures was performed with REFMAC5 (8) and PHENIX.REFINE (9). Manual model building was carried out using COOT (10). Validation of the obtained model was performed with tools within COOT as well as PROCHECK (11), SFCHECK (12) and MOLPROBITY (13). Ligands were included for refinement when they were visible in the electron density maps. Ligand restraint files were generated with the Grade Web Server (Smart, O. S., T. O.Womack, A. Shar, C. Flensburg, P. Keller, W. Paciorek, C. Vonrhein and G. Bricogne (2011). Grade, version 1.2.7. http://www.globalphasing.com.). The PHENIX suite was used to create simulated annealing omit maps. Structural representations were designed with PyMOL (Schrödinger).

Enzyme activity. Enzyme activity was monitored spectrophotometrically at 50 °C by HSCoA liberation using Ellman´s thiol reagent (DTNB) (14). The assay contained 100 mM MES/NaOH pH 7.0, 0.1 mM DTNB, 5 mM $MgCl_2$, 1 mM of either ADP or GDP, 0.1 mM acetyl-CoA, 20 mM KH_2PO_4. For determination of K_m values, the concentration of ADP and GDP was varied between 0 and 2 mM.

Generation of kcr_0115 mutants. The *ckc*ACD1-H68A and *ckc*ACD1-H68N mutants of the beta subunit were generated using the QuikChange II XL protocol (Stratagene) according to the manufacturer's manual. The primers used to introduce the mutations were 5´-

TATCCCCTCAAGTGGTCGCTAAAAGCGATGTGGGCG-3′ (forward) together with 5′-CGCCCACATCGCTTTTAGCGACCACTTGAGGGGATA-3′ (reverse) for generation of pET17bkcr_0115H69A (*ckc*ACD1-H68A) and 5′-TATCCCCTCAAGTGGTCAAT-AAAAGCGATGTGGGC-3′ (forward) together with 5′-GCCCACATCGCTTTTATT-GACCACTTGAGGGGATA-3′ (reverse) for generation of pET17bkcr_0115H69N (*ckc*ACD1-H68N). *E. coli* BL21(DE3) RIL cell pellets, transformed with pET17bkcr_0115 or pET17bkcr_0198, respectively, and *E. coli* Rosetta (DE3) pLysS cell pellets transformed with pET17bkcr_0115H69A or pET17bkcr_0115H69N, respectively, were suspended in TRIS/HCl, pH 8.85 containing 5 mM $MgCl_2$ and disrupted by sonication. Supernatant was heat-precipitated at 85 °C for 20 min and precipitated proteins were removed by centrifugation. Subunits were reconstituted and applied to a Superdex 200 16/60 column equilibrated with 50 mM TRIS/HCl, pH 7.5, containing 150 mM NaCl. Protein was eluted at a flow rate of 1 ml min^{-1}, yielding pure protein.

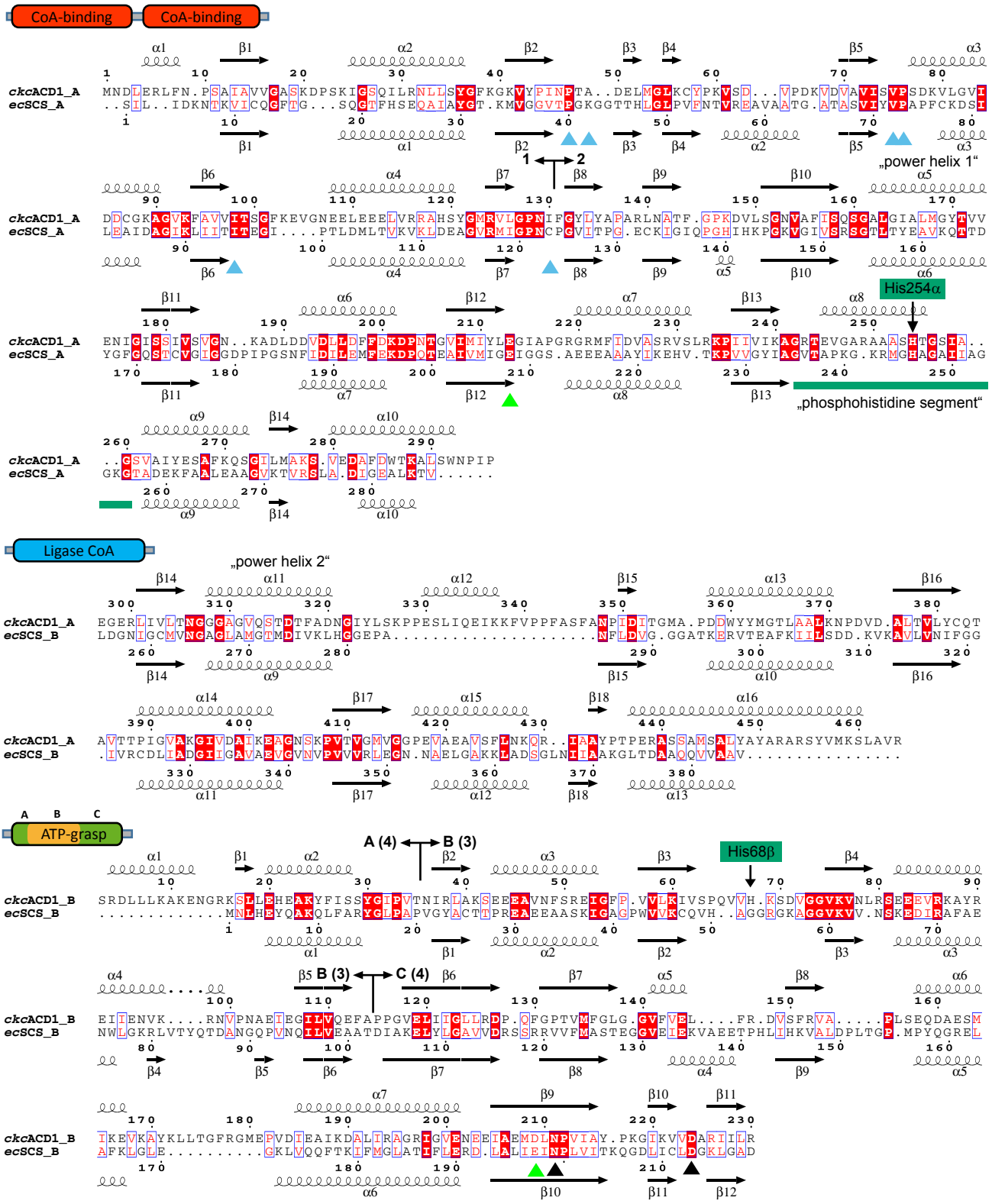
CoA-binding
CoA-binding
ckcACD1_A
ecSCS_A
„power helix 1“
His254α
„phosphohistidine segment“
Ligase CoA
„power helix 2“
ckcACD1_A
ecSCS_B
A B C
ATP-grasp
A (4) B (3)
His68β
B (3) C (4)
ckcACD1_B
ecSCS_B

Fig. S1. Sequence alignment of *ckc*ACD1 with *ec*SCS. The sequence alignment is based on superimposed structures using the program GESAMT (15). Since due to domain shuffling the order of individual domains is rearranged, equivalent domains are individually aligned. The respective domain notation is given. Residues of *ec*SCS which are known to be important for catalysis are marked by a triangle in green (16, 17) (*ec*SCS-residues: His246α, Glu208α – interacting with His246α, Glu197β – mostly Asp in other family members). Residues interacting with coenzyme A (CoA) are marked by a triangle in blue (18)(*ec*SCS residues: Pro40α, Lys42α, Val72α, Pro73α, Ile95α and Cys123α). Residues coordinating the magnesium ion of the ADP-binding site within the ATP-grasp domain are marked by a triangle in black (*ckc*ACD1 residues: Asn211β and Asp224β). The phosphohistidine segment with the phosphorylated histidine residue His254α is underlined in green. The second, highly conserved histidine residue His68β known to be important for catalysis in *ckc*ACD1 is highlighted in green. The "power helices" defining the phosphate binding site I are labeled (*ec*SCS α5(α-subunit) and α9(β-subunit); *ckc*ACD1 α5(α-subunit) and α11(α'-subunit)). The " ' " indicates the symmetry mate within the $\alpha_2\beta_2$-heterotetramer. The subdivision in three domains (A, B, and C) for the ATP-grasp domain is in accordance to Fawaz *et al.* (19). The hinge region for the lid-domain B of the ATP-grasp domain (beta subunit in *ckc*ACD1 and subdomain 3-4 in *ec*SCS) is located at the two changeovers from one domain to the other as indicated (A←→ B and B ←→ C, respectively).

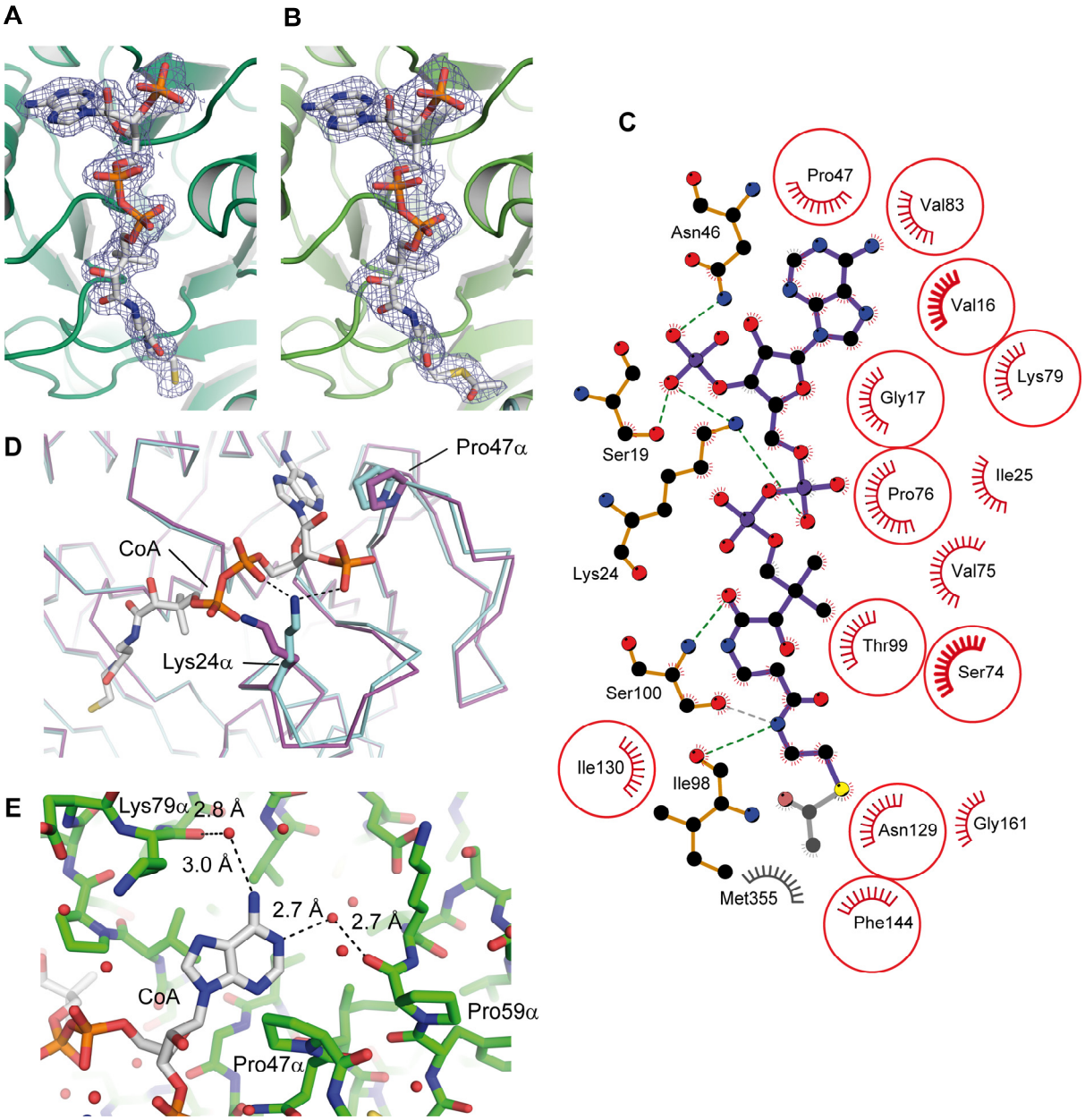

Fig. S2. Binding mode of (acetyl-)CoA within the alpha subunit. Electron density map defining the position of the bound cofactor CoA (**A**) and acetyl-CoA (**B**). Carbon atoms in acetyl-CoA are shown in white, nitrogen in blue, oxygen in red, phosphor in orange, and sulfur in yellow. Density is contoured at 1.0σ (blue mesh). The electron density distribution was calculated without the presence of the cofactor. The surrounding protein is displayed as cartoon representation in green. The binding mode is identical for the main part of the cofactor. (**C**) Schematic representation of the binding environment for acetyl-CoA as calculated with the program LigPlot (20). (**D**) Only small conformational adaptions where observed upon CoA binding in comparison to the cofactor free apoenzyme. The sidechain of Lys24α becomes oriented between the 3‘- and 5‘- phosphate groups of CoA. Due to hydrophobic interactions of

the adenosine moiety with the protein, a small closure of the pocket is observed around residue Pro47α. (**E**) Orientation of the adenosine group of CoA in the hydrophobic pocket is facilitated by interaction with water molecules (red spheres) coordinated to the main chain carbonyl group of Pro59α and Lys79α, respectively.

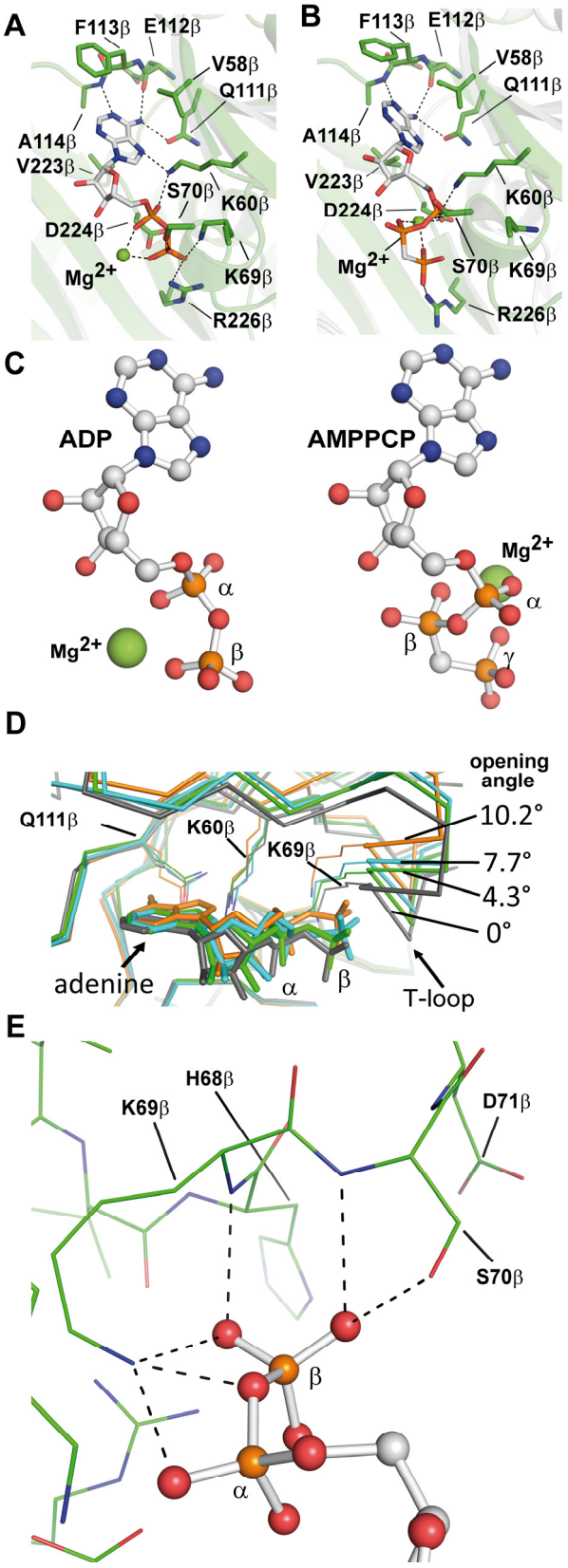

Fig. S3. Binding of nucleotides within the ATP-grasp domain of the beta subunit. Residues interacting with (A) ADP (crystal structure *ckc*ACD1-D) and (B) AMPPCP (crystal structure *ckc*ACD1-C). Carbon atoms in the nucleotides are shown in white, nitrogen in blue, oxygen in

red, and phosphor in orange. (C) Orientation of the phosphate groups of ADP and AMPPCP, respectively, based on the superposition of the adenine and sugar moiety. The green spheres represent magnesium ions, which are complexed by the phosphate groups. (D) Opening of the ATP-grasp domain due to the movement of the lid domain causes changes of the adenosine diphosphate binding. Shown is a superposition of the ATP-grasp domains of the crystal structures *ckc*ACD1-B (grey), *ckc*ACD1-D (green), *ckc*ACD1-H (blue), and *ckc*ACD1-G (orange). (E) Interaction of the beta phosphate group of ADP with the T-loop (Lys60β-Val75β). Depicted is the crystal structure of *ckc*ACD1-D. Several hydrogen bonds (black dashes) are observed, which facilitate strong interactions between the protein and the phosphate moiety.

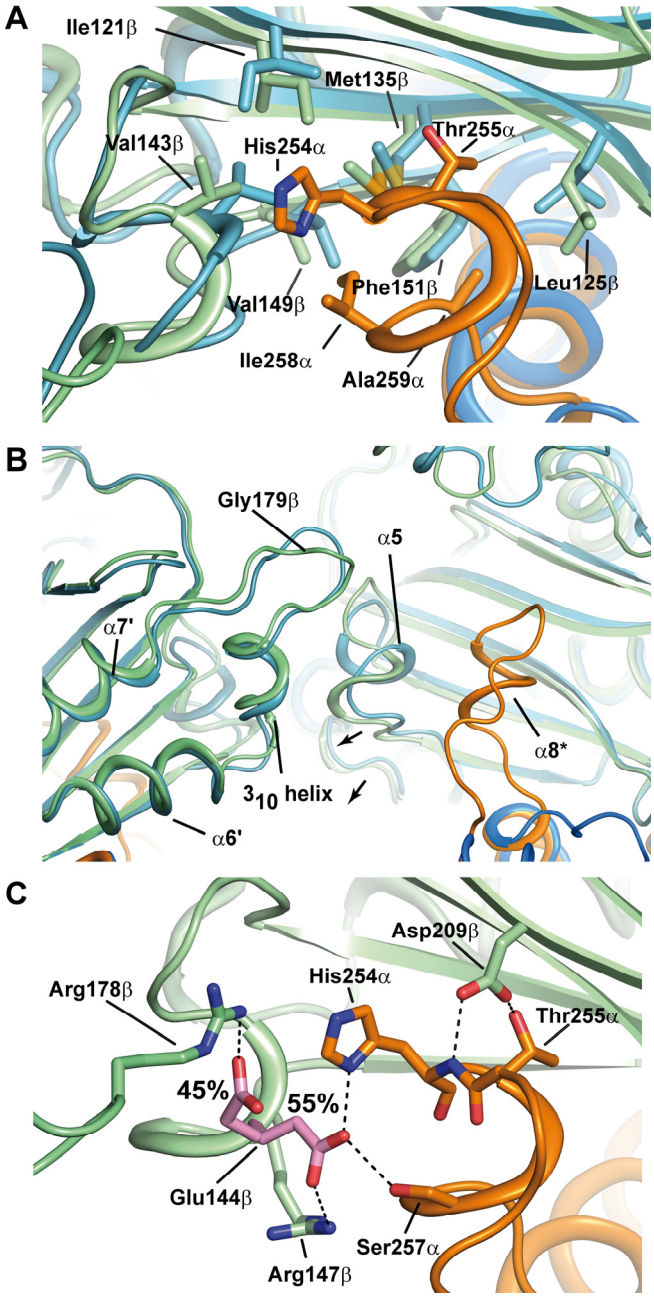

Fig. S4. (**A**) Interaction of the phosphohistidine segment (orange) with the ATP-grasp domain of the beta subunit causes rearrangements. Depicted are the ATP-grasp domain of *ckc*ACD1-B (blue; phosphohistidine segment positioned towards binding site I (see as well **Fig. 3** and **Fig. 4**)) and *ckc*ACD1-C (orange; phosphohistidine segment swung towards binding site II (see as well **Fig. 4** and **Fig. 5**)). Residues from the lid domain are omitted for clarity. (**B**) Formation of a hydrophobic pocket results in reorganization of helix α5 and subsequently in relocation of the residues between the helices α6' and α7'. Arrows indicate the direction of the movement within the ATP-grasp domain. (**C**) Two conformers for the glutamate residue Glu144β (carbon atoms in magenta and oxygen atoms in red) are observed in the crystal structure *ckc*ACD1-C. The value noted next to the conformers are the refined occupancies as observed in the crystal structure. Conformer A (55%) of Glu144β is involved in hydrogen bonds with the phosphohistidine segment side chains His254α and Ser257α (carbon atoms in orange, nitrogen atoms in blue, and oxygen atoms in red). In addition, an ionic interaction to the guanidine group of Arg147β is observed. The conformer B (45%) forms a salt bridge to the guanidine group of Arg178β'. Depicted is also residue Asp209β (carbon atoms in green and oxygen atoms in red). This residue stabilizes the phosphohistidine segment via hydrogen bonds to the side chain of Thr255α and the backbone nitrogen of His254α. Residues from the lid domain are omitted for clarity.

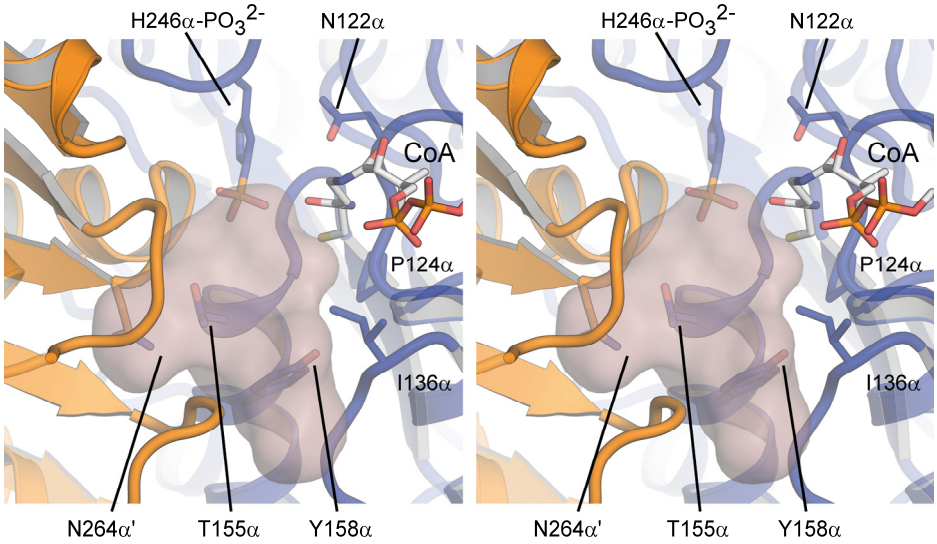

Fig. S5. Binding site for activated acyl-moiety. Stereo representation of the proposed binding pocket for the succinyl group as defined by the *ec*SCS structure (PDB entry 2SCU (18)).

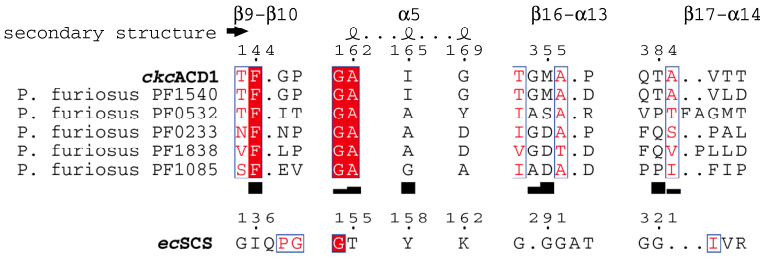

Fig. S6. Sequence variations within the substrate binding region determines substrate selectivity. Multiple sequence alignment of *ckc*ACD1, *ec*SCS and five isoforms of the ACDs from *P. furiosus*. The converted substrates for the different *pf*ACDs are well characterized (21). The potential involvement of individual residues on substrate recognition are based on the interpretation of the obtained structures of *ckc*ACD1 and the importance is highlighted as black bar.

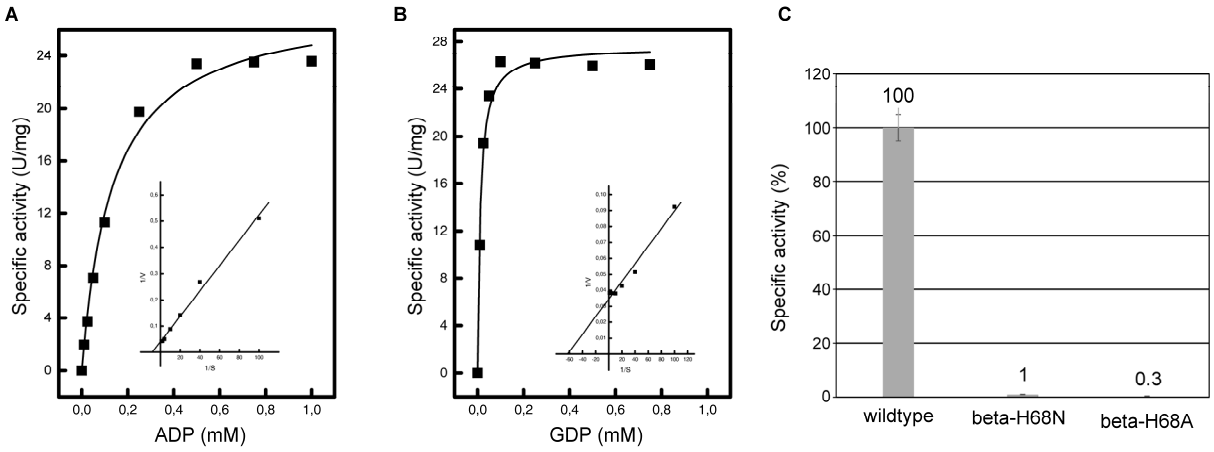

Fig. S7. Enzymatic activity of wild type and mutant *ckc*ACD1.The determination of the rate dependency of recombinant *ckc*ACD1 on ADP (*A*) and GDP (*B*) revealed that *ckc*ACD1 could use ADP as well as GDP as substrate for the activated phosphate. The inserts show the double-reciprocal plots of the rates against the corresponding substrate concentrations. The determined K_m and V_{max} values are 0.1 mM and 24-25 U/mg for ADP (duplicate measurement), respectively, and 0.04 mM and 29-32 U/mg for GDP (triplicate measurement), respectively. (*C*) His68β is crucial for *ckc*ACD1 activity to generate ATP. Levels of acetate-forming activity of wildtype and beta subunit variants of recombinant *ckc*ACD1 are given in percent activity. Specific activity of wildtype (50 U/mg) is set as 100 % activity. The mutant proteins *ckc*ACD1-

H68N (beta-H68N) and *ckc*ACD1-H68A (beta-H68A) have only residual activities of 0.5 U/mg and 0.15 U/mg, respectively. Given error bars indicate standard deviation of 5 to 8 measurements (wildtype = 4.89 U/mg, beta-H68N = 0.18 U/mg, beta-H68A = 0.08 U/mg). Measurements were performed at 85 °C.

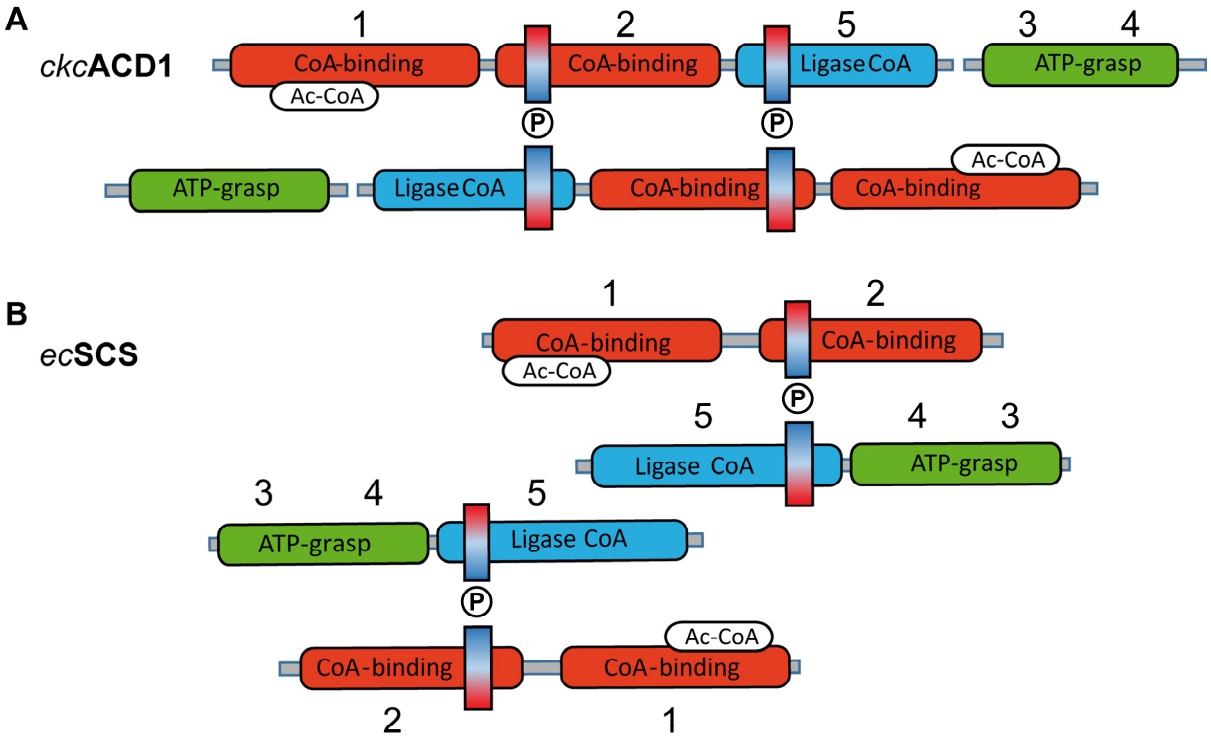

Fig. S8. The domain arrangement of *ckc*ACD1 requires a heterotetrameric $\alpha_2\beta_2$ complex for activity. Scheme of domain arrangement and heterocomplex formation of *ckc*ACD1 (*A*) and *ec*SCS (*B*). The color code for the individual subdomains is the same as used for **Fig. 1 and SI, Fig. S1**. The boxes represent the two power helices, which stabilize the phosphate moiety within the active site I.

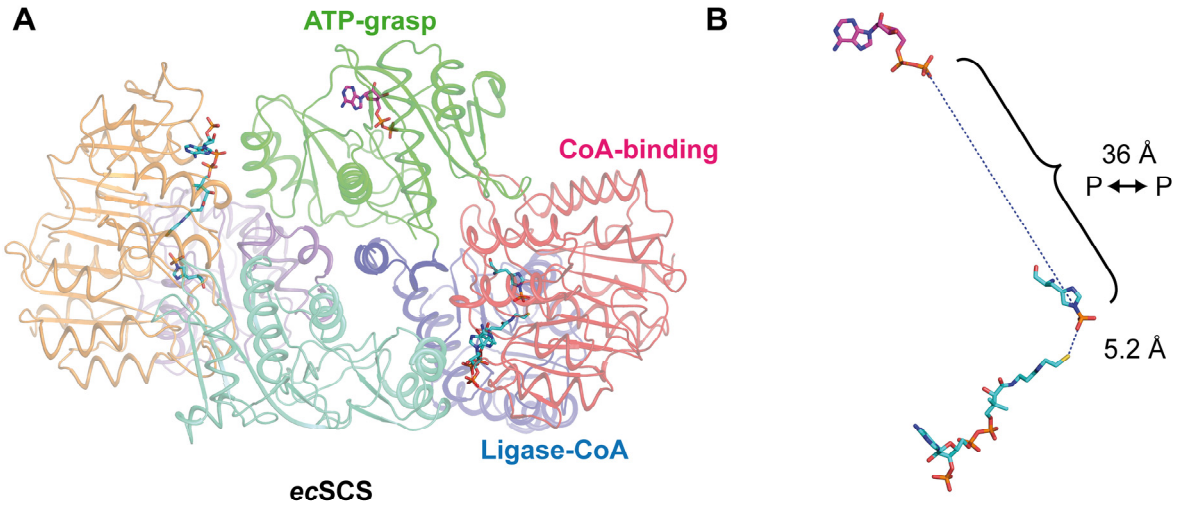

Fig. S9. For the heterotetrameric *ec*SCS a swinging-loop mechanism is proposed. (*A*) Depiction of the arrangement of the five subdomains within *ec*SCS (color scheme in accordance to **Fig. 1)**. The cofactor CoA and the final substrate ADP are shown in stick representation. (*B*) Distance between phosphorylated histidine and CoA (carbon atoms in cyan, nitrogen atoms in blue, phosphor atoms in orange, sulfur atom in yellow, and oxygen atoms in red) oriented towards site I and ADP bound at site II (carbon atoms in magenta, nitrogen atoms in blue, phosphor atoms in orange, and oxygen atoms in red). Representation is based on PDB-entries 2SCU (18) and 1CQJ (22).

The alpha domain features an additional nucleotide binding site. In the electron density of *ckc*ACD1-D and *ckc*ACD1-C, clear evidence for an additionally bound ADP and AMPPCP molecule, respectively, was identified. We observed this only in data collected from crystals grown at 278 K, which indicate an artificial origin. Thus, this observation has most likely no physiological relevance. The terminal phosphate groups of both ADP and AMPPCP facilitate the binding to the alpha domain. In case of ADP, the adenine moiety interacts in addition via π-π-stacking with the imidazole group of His254α. We did not observe electron density for the adenine moiety of AMPPCP. In both cases, we identified an additionally bound metal ion, presumably a magnesium ion, in octahedral coordination through one oxygen atom of the phosphate group as well as five surrounding water molecules (**SI, Fig. S4**). Two of these water molecules are furthermore coordinated to the carboxyl group of Asp351α'. Interestingly, a similar interaction of water molecules with Asp351α' could be observed as well in the crystal structures of *ckc*ACD1 with phosphorylated His254α (*ckc*ACD1-H) and in complex with a

phosphate ion (*ckc*ACD1-G) (**Fig. 3**). This aspartate residue is extraordinarily conserved in all ACDs and SCS (**SI, Fig. S1** and (23)). Hence, we propose that this residue and the observed phosphate binding motif might play an important role in the enzymatic function of ACDs.

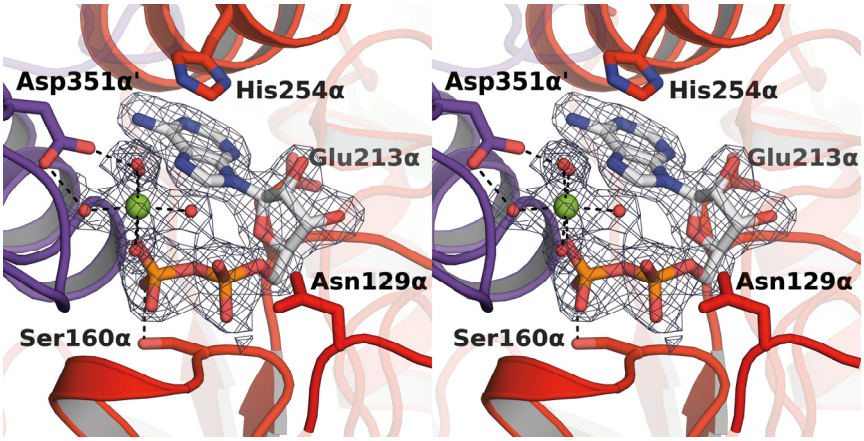

Fig. S10. ADP-binding site within the alpha subunit. Stereo representation of the omit electron density map used to define the position of ADP within the alpha subunit (blue mesh, density is contoured at 1.0σ). ADP as well as interacting residues are represented as sticks (carbon atoms in white, nitrogen atoms in blue, phosphor atoms in orange, and oxygen atoms in red). The bound magnesium ion is shown as green sphere and the coordinating water molecules are shown as red spheres.

Table S1. Data collection and refinement statistics.

***ckc*ACD1-#**	**A**	**B**	**C**	**D**	**E**	**F**	**G**	**H**	**I**
PDB entry	4XYL	4XYM	4XZ3	4Y8V	4YAK	4YAJ	4YB8	4YBZ	5HBR
Data collection[1]									
Synchrotron X-ray source	PETRAIII P14	PETRAIII P14	BESSY BL14.1	BESSY BL14.1	PETRAIII P14 & BESSY BL14.1	BESSY BL14.1	PETRAIII P14	PETRAIII P14	PETRAIII P14
Wave length (Å)	1.24	1.24	0.98	0.98	0.98	0.98	0.98	0.98	0.98
Resolution range (Å)	83.46-1.95 (1.98-1.95)	127.04-1.90 (1.93-1.90)	48.84-2.40 (2.47-2.40)	49.21-2.10 (2.14-2.10)	83.57-2.46 (2.53-2.46)	125.81-2.20 (2.25-2.20)	110.61-1.90 (1.93-1.90)	83.03-2.10 (2.14-2.10)	126.03-1.99 (2.03-1.99)
Space group	$P2_12_12_1$	$P2_12_12_1$	$P2_12_12_1$	$P2_12_12_1$	$P2_12_12_1$	$P2_12_12_1$	$P2_12_12_1$	$P2_12_12_1$	$P2_12_12_1$
Unit cell a, b, c (Å)	102.5, 112.2, 124.9	99.6, 114.4, 127.0	100.2, 111.9, 127.6	106.5, 111.0, 126.7	106.4, 111.7, 126.0	105.8, 111.2, 125.8	106.1, 110.6, 125.7	105.3, 109.9, 126.8	106.1, 110.7, 126.0
Total reflections	684725 (33884)	706193 (8766)	711978 (56845)	548838 (15840)	591856 (23566)	570073 (7989)	1515778 (55680)	573438 (30751)	672786 (27311)
Unique reflections	105037 (5118)	112092 (3230)	56770 (4557)	86108 (3595)	54078 (3442)	73935 (2617)	116787 (5673)	85835 (4477)	101504 (4632)
Multiplicity	6.5 (6.6)	6.3 (2.7)	12.5 (12.5)	6.4 (4.4)	10.9 (6.8)	7.7 (3.1)	13.0 (9.8)	6.7 (6.9)	6.6 (5.9)
Completeness (%)	99.8 (99.7)	97.8 (58.1)	99.9 (98.8)	97.6 (77.9)	98.1 (77.3)	97.3 (57.0)	100.0 (99.5)	99.5 (99.1)	99.6 (93.1)
Mean I/σ(I)	6.7 (0.6)	8.1 (0.3)	9.9 (0.8)	10.1 (1.1)	9.7 (0.6)	6.4 (0.4)	9.4 (0.5)	7.5 (0.8)	8.4 (0.5)
CC(1/2)	0.992 (0.169)	0.996 (0.103)	0.995 (0.229)	0.995 (0.422)	0.996 (0.231)	0.990 (0.105)	0.998 (0.159)	0.993 (0.312)	0.998 (0.124)
Wilson *B*-factor ($Å^2$)	25.5	24.9	40.2	20.4	45.3	30.8	37.1	26.2	37.2
Refinement									
R-work (%)	20.64	19.53	19.65	18.44	19.36	21.45	18.16	21.58	17.84
R-free (%)	24.64	23.71	24.44	22.55	23.82	24.13	22.05	25.34	22.22
CC* (24)	0.998	0.999	0.999	0.999	0.999	0.998	0.999	0.998	0.999
CC-work (24)	0.955	0.961	0.960	0.967	0.973	0.961	0.975	0.939	0.975
CC-free (24)	0.938	0.952	0.944	0.945	0.948	0.939	0.966	0.909	0.956
B-factors ($Å^2$) (nonhydrogen atoms) (25)									
All	36.7 (10886)	39.5 (11074)	60.70 (10550)	33.6 (11131)	64.2 (10559)	43.9 (10359)	47.9 (10782)	41.8 (10972)	52.2 (10944)
Main chain	35.5 (5508)	37.7 (5532)	56.9 (5461)	31.7 (5544)	62.5 (5516)	42.7 (5432)	46.0 (5544)	40.2 (5532)	50.1 (5544)
Side chain	38.3 (4916)	41.6 (4939)	62.9 (4826)	35.4 (4956)	66.2 (4926)	45.7 (4754)	50.1 (4876)	43.6 (4950)	55.0 (4951)
solvent	32.5 (364)	38.4 (436)	45.0 (56)	31.1 (519)	50.5 (18)	35.1 (171)	42.2 (293)	40.5 (461)	46.2 (340)

ADP				55.5 (54)			78.3 (54)	68.8 (27)	
ADP*				53.8 (54)					
AMPCP		40.7 (54)							
AMPPCP			97.0 (62)						
AMPPCP*			82.8 (44)						
CoA	33.6 (96)	40.2 (96)	62.1 (96)		58.8 (48)				49.9 (96)
AcCoA					63.0 (51)				
Phosphate							52.6 (10)		54.3 (10)
Estimated coordinate error (Å)	0.29	0.32	0.38	0.25	0.44	0.27	0.30	0.31	0.30
rmsd (bonds) (Å) (26)	0.005	0.007	0.004	0.004	0.006	0.003	0.012	0.004	0.008
rmsd (angle) (°) (26)	0.940	1.056	0.763	0.921	0.880	0.771	1.201	0.970	1.047
Molprobity all-atom clashscore (27)	2.22	2.20	1.81	1.64	2.78	0.83	2.61	2.79	2.15
Rotamer outliers (%)	2.16	0.71	1.04	1.78	2.61	1.12	0.54	2.42	2.50
Ramachandran plot statistics (%)									
Favoured	97.95	97.82	96.60	98.26	97.30	97.02	97.75	97.75	97.68
Allowed	1.90	2.04	3.25	1.60	2.56	2.83	2.10	2.11	2.18
Outliers	0.15	0.15	0.15	0.15	0.15	0.15	0.15	0.15	0.15

Parameters for the outermost shell are shown in parentheses. CC(1/2), percentage of correlation between intensities from random half datasets. Correlation significant at the 0.1 % level (24). CC*, the CC of the full dataset against the true intensities (24). R-work, $R=100 \times \sum_{hkl} \big| |F_{obs}| - |F_{calc}| \big| / \sum_{hkl} |F_{obs}|$, where F_{obs} and F_{calc} are the observed and calculated structure-factor amplitudes, respectively; R-free is equivalent to R-work but is calculated from reflections (5%) that were omitted from the refinement process (28, 29). Description of *B*-factors: values in parentheses corresponds to the number of atoms. Nucleotides marked with an asterisk are bound to the alpha subunit.

Table S2. Opening angle within the ATP-grasp domain of the beta subunit of *ckc*ACD1.

Crystal structure	α-β	α‘-β‘
ACD1-A	0.0 ° §	1.5 °
ACD1-B	23.8 °	13.7 °
ACD1-C	16.6 °	9.3 °
ACD1-D	9.3 °	4.3 °
ACD1-E	18.2 °	12.2 °
ACD1-F	10.8 °	9.3 °
ACD1-G	10.2 °	4.6 °
ACD1-H	12.7 °	7.7 °
ACD1-I	24.6 °	10.2 °

§ The crystal structure *ckc*ACD1-B was set as the reference for the ‚closed‘ conformation. Its opening angle was set to 0.0 °. For the determination of the opening angle the relative orientation of the lid domain (subdomain 3, residues Thr35β – Phe113β) was compared with the subdomain 4 (residues Ser3β – Pro33β / Gly117β – Arg230β) **(**see **Fig. 1**).

Reference List

1. Gasteiger, E., Hoogland, C., Gattiker, A., Duvaud, S., Wilkins, M. R., ppel, R. D., & airoch, A. (2005) in *The Proteomics Protocols Handbook*, ed. Joh M.Walker (Humana Press, pp. 571-607.

2. Mueller U, Darowski N, Fuchs MR, Forster R, Hellmig M, Paithankar KS, Puhringer S, Steffien M, Zocher G, Weiss MS (2012) Facilities for macromolecular crystallography at the Helmholtz-Zentrum Berlin. *J. Synchrotron. Radiat.* 19(Pt 3): 442-449.

3. Kabsch W (2010) XDS. *Acta Crystallogr. D. Biol. Crystallogr.* 66(Pt 2): 125-132.

4. Evans PR, Murshudov GN (2013) How good are my data and what is the resolution? *Acta Crystallogr. D. Biol. Crystallogr.* 69(Pt 7): 1204-1214.

5. Schwede T, Kopp J, Guex N, Peitsch MC (2003) SWISS-MODEL: An automated protein homology-modeling server. *Nucleic Acids Res.* 31(13): 3381-3385.

6. Vagin A, Teplyakov A (1997) MOLREP: An automated programm for molecular replacement. *J. Appl. Cryst.* 30 1022-1025.

7. Adams PD, Afonine PV, Bunkoczi G, Chen VB, Davis IW, Echols N, Headd JJ, Hung LW, Kapral GJ, Grosse-Kunstleve RW *et al.* (2010) PHENIX: a comprehensive Python-based system for macromolecular structure solution. *Acta Crystallogr. D. Biol. Crystallogr.* 66(Pt 2): 213-221.

8. Murshudov GN, Skubak P, Lebedev AA, Pannu NS, Steiner RA, Nicholls RA, Winn MD, Long F, Vagin AA (2011) REFMAC5 for the refinement of macromolecular crystal structures. *Acta Crystallogr. D. Biol. Crystallogr.* 67(Pt 4): 355-367.

9. Afonine PV, Grosse-Kunstleve RW, Echols N, Headd JJ, Moriarty NW, Mustyakimov M, Terwilliger TC, Urzhumtsev A, Zwart PH, Adams PD (2012) Towards automated crystallographic structure refinement with phenix.refine. *Acta Crystallogr. D. Biol. Crystallogr.* 68(Pt 4): 352-367.

10. Emsley P, Lohkamp B, Scott WG, Cowtan K (2010) Features and development of Coot. *Acta Crystallogr. D. Biol. Crystallogr.* 66(Pt 4): 486-501.

11. Laskowski RA, MacArthur MW, Moss DS, Thornton JM (1993) PROCHECK: a program to check the stereochemical quality of protein structures. *J. Appl. Cryst.* 26 283-291.

12. Vaguine AA, Richelle J, Wodak SJ (1999) SFCHECK: a unified set of procedures for evaluating the quality of macromolecular structure-factor data and their agreement with the atomic model. *Acta Crystallogr. D. Biol. Crystallogr.* 55(Pt 1): 191-205.

13. Chen VB, Arendall WB, III, Headd JJ, Keedy DA, Immormino RM, Kapral GJ, Murray LW, Richardson JS, Richardson DC (2010) MolProbity: all-atom structure validation for macromolecular crystallography. *Acta Crystallogr. D. Biol. Crystallogr.* 66(Pt 1): 12-21.

14. Ellman GL (1958) A colorimetric method for determining low concentrations of mercaptans. *Arch. Biochem. Biophys.* 74(2): 443-450.

15. Krissinel E, Henrick K (2007) Inference of macromolecular assemblies from crystalline state. *J. Mol. Biol.* 372(3): 774-797.

16. Majumdar R, Guest JR, Bridger WA (1991) Functional consequences of substitution of the active site (phospho)histidine residue of Escherichia coli succinyl-CoA synthetase. *Biochim. Biophys. Acta* 1076(1): 86-90.

17. Fraser ME, Joyce MA, Ryan DG, Wolodko WT (2002) Two glutamate residues, Glu 208 alpha and Glu 197 beta, are crucial for phosphorylation and dephosphorylation of the active-site histidine residue in succinyl-CoA synthetase. *Biochemistry (Mosc).* 41(2): 537-546.

18. Fraser ME, James MN, Bridger WA, Wolodko WT (1999) A detailed structural description of *Escherichia coli* succinyl-CoA synthetase. *J. Mol. Biol.* 285(4): 1633-1653.

19. Fawaz MV, Topper ME, Firestine SM (2011) The ATP-grasp enzymes. *Bioorg. Chem.* 39(5-6): 185-191.

20. Wallace AC, Laskowski RA, Thornton JM (1995) LIGPLOT: a program to generate schematic diagrams of protein-ligand interactions. *Protein Eng* 8(2): 127-134.

21. Scott JW, Poole FL, Adams MW (2014) Characterization of ten heterotetrameric NDP-dependent acyl-CoA synthetases of the hyperthermophilic archaeon *Pyrococcus furiosus*. *Archaea.* 2014 176863.

22. Joyce MA, Fraser ME, James MN, Bridger WA, Wolodko WT (2000) ADP-binding site of *Escherichia coli* succinyl-CoA synthetase revealed by X-ray crystallography. *Biochemistry (Mosc).* 39(1): 17-25.

23. Sanchez LB, Galperin MY, Muller M (2000) Acetyl-CoA synthetase from the amitochondriate eukaryote *Giardia lamblia* belongs to the newly recognized superfamily of acyl-CoA synthetases (Nucleoside diphosphate-forming). *J. Biol. Chem.* 275(8): 5794-5803.

24. Karplus PA, Diederichs K (2012) Linking crystallographic model and data quality. *Science* 336(6084): 1030-1033.

25. Popov AN, Bourenkov GP (2003) Choice of data-collection parameters based on statistic modelling. *Acta Crystallogr. D. Biol. Crystallogr.* 59(Pt 7): 1145-1153.

26. Engh RA, Huber R (1991) Accurate bond and angle parameters for X-ray protein structure refinement. *Acta Crystallogr.* A47 392-400.

27. Davis IW, Leaver-Fay A, Chen VB, Block JN, Kapral GJ, Wang X, Murray LW, Arendall WB, III, Snoeyink J, Richardson JS *et al.* (2007) MolProbity: all-atom contacts and structure validation for proteins and nucleic acids. *Nucleic Acids Res.* 35(Web Server issue): W375-W383.

28. Tickle IJ, Laskowski RA, Moss DS (2000) R_{free} and the R_{free} ratio. II. Calculation of the expected values and variances of cross-validation statistics in macromolecular least- squares refinement. *Acta Crystallogr. D.* 56 (Pt 4) 442-450.

29. Brunger AT (1992) Free R value: a novel statistical quantity for assessing the accuracy of crystal structures. *Nature* 355 472-475.